

# Size-dependent ultrafast structural dynamics inside phospholipid vesicle bilayers measured with 2D IR vibrational echoes

Oksana Kel, Amr Tamimi, and Michael D. Fayer<sup>1</sup>

Department of Chemistry, Stanford University, Stanford, CA 94305

Contributed by Michael D. Fayer, December 15, 2013 (sent for review November 25, 2013)

**The ultrafast structural dynamics inside the bilayers of dilauroyl-phosphatidylcholine (DLPC) and dipalmitoylphosphatidylcholine vesicles with 70, 90, and 125 nm diameters were directly measured with 2D IR vibrational echo spectroscopy. The antisymmetric CO stretch of tungsten hexacarbonyl was used as a vibrational probe and provided information on spectral diffusion (structural dynamics) in the alkyl region of the bilayers. Although the CO stretch absorption spectra remain the same, the interior structural dynamics become faster as the size of the vesicles decrease, with the size dependence greater for dipalmitoylphosphatidylcholine than for DLPC. As DLPC vesicles become larger, the interior dynamics approach those of the planar bilayer.**

vesicle bilayer dynamics | vesicle size dependent dynamics | vesicles chainlength dependent dynamics

The plasma membrane provides a boundary between a living cell and its surroundings and between cellular compartments, providing organizational control of proteins and small molecules that are critical for achieving the complexity of biological systems. In addition to a permeability barrier, the second role of the plasma membrane is serving as the solvent for membrane proteins and other biomolecules. The lipid environment of membrane proteins can influence their function (1–5), and so impact cell signaling, metabolism, growth, defense, and a myriad of other biological functions.

Membranes have a bilayer structure where the nonpolar chains of the lipids form the interior of bilayer, with zwitterionic or ionic head groups at the interfaces with water. Artificial lipid bilayers are frequently used as models of cell membranes for investigation of membrane properties and in studies of transmembrane proteins. Although a good deal is known about the structure of artificial membranes (6–12) and orientational and translational diffusion of lipids and other molecules (7, 13–16), much less is known about the fast interior structural dynamics of the bilayers, which serve as the dynamic bath modes that can impact membrane processes.

Unilamellar vesicles (ULVs) of different sizes, as well as multilamellar vesicles (MLVs), are used as model membranes owing to their ease of preparation and handling. It has been shown that their properties depend on the curvature (size) (8, 9, 13, 17–20). Aligned planar multi-bilayers (21) are membrane models that do not have curvature, yet they are less attractive for routine use because they are substantially more difficult to prepare than vesicles.

Numerous experiments have been performed to determine which type of model bilayers most closely represents the properties of the plasma membrane. However, no consensus exists because the results obtained by different methods and groups are not in agreement. Some small-angle X-ray scattering and small-angle neutron scattering (SANS) experiments indicate that the structural properties of ULVs and MLVs are curvature independent, the overall bilayer thickness does not depend on vesicle size, and the thicknesses of inner and outer leaflets of the bilayer are indistinguishable (6, 22). Other SANS experiments, supported by

computer simulations (7), reported curvature dependent structural changes, with a decrease of the bilayer thickness with increasing vesicle size (8, 9). In contrast, other calculations showed that bilayers become thicker with increasing vesicle size, but with no difference in thickness of inner and outer leaflets for vesicles of different sizes (10). Other research reported an asymmetrical geometry and that the thickness of the outer leaflet is greater than that of the inner (11, 12). The thermodynamic properties of lipid bilayers can also depend on the type of the model membrane. It has been reported that a decrease in vesicle size leads to an increase in the enthalpy of formation (17), and that diffusion coefficients inside the vesicle bilayer are size dependent, with small vesicles having larger diffusion coefficients (13). In contrast, molecular dynamics (MD) simulations pointed to an increasing diffusion coefficient with increasing vesicles size with the highest value for planar bilayers (7). Other properties, such as fusion rate (18, 23), phase transition temperature (19, 24, 25), and elasticity (20), have been shown to vary for vesicles of different sizes.

NMR studies can provide a great deal of information on bilayer dynamics and order parameters. They have been used to investigate the effect of vesicle curvature on the dynamics of lipid acyl chains. However, the results of various studies are not always consistent. Some groups have shown that curvature (vesicle size) does not influence the rates of lipid motions (26–29) whereas others have provided evidence that there are significant changes with vesicle diameter (14–16). These are complex experiments, particularly when they recover information on ultrafast time scales that reflect structural fluctuations in contrast to slower processes of translational and orientational diffusion. Complex line-shape fitting is used that requires parameters that may not be possible to determine precisely. In contrast with some of the NMR studies, MD simulations indicate that reorientation times

## Significance

**Plasma membranes hold a wide variety of proteins and other biomolecules that are essential to cell functions. In addition, membranes are the solvent bath, which is intimately coupled to transmembrane processes. Membranes are frequently modeled using planar phospholipid bilayers and vesicles. However, vesicles are small and have relatively small radii of curvature. Research has shown that the bilayer curvature influences structural and thermodynamic properties, but much less is known about the interior dynamics of model membranes. Here we address ultrafast structural dynamics inside vesicle and planar bilayers using 2D IR vibrational echo experiments. The results show that the interior dynamics depend on the phospholipid chain length and are curvature dependent, with the dynamics becoming faster as the vesicle size decreases.**

Author contributions: O.K. and M.D.F. designed research; O.K., A.T., and M.D.F. performed research; O.K., A.T., and M.D.F. analyzed data; and O.K. and M.D.F. wrote the paper.

The authors declare no conflict of interest.

<sup>1</sup>To whom correspondence should be addressed. E-mail: fayer@stanford.edu.

of the lipid tails become faster with increasing vesicle size and that planar bilayers have the fastest reorientation dynamics (7).

In this article we address the ultrafast structural dynamics of the vesicle bilayers composed of dilauroylphosphatidylcholine (DLPC) or dipalmitoylphosphatidylcholine (DPPC) phospholipids, which differ in the length of alkyl chains. Ultrafast 2D IR vibrational echo experiments were used to examine the dynamics in the alkyl chain interiors of phospholipid vesicle bilayers. The experiments directly report on the time dependence of the structural fluctuation of the bilayers by measuring spectral diffusion. This method is very sensitive to structural changes, provides femtosecond time resolution, and can explicate the ultrafast dynamics of vesicle bilayers.

The experiments were performed on the antisymmetric stretching mode of tungsten hexacarbonyl [ $W(CO)_6$ ].  $W(CO)_6$  was selected as the vibrational probe for several reasons. First, it is a nonpolar hydrophobic molecule that locates preferentially in the bilayer interiors (30). In addition,  $W(CO)_6$  has a long vibrational lifetime, making it possible to observe dynamics over a range of times from 300 fs to 200 ps.  $W(CO)_6$  is substantially smaller than DLPC and even smaller than DPPC.  $W(CO)_6$  has a molecular volume of  $\sim 100 \text{ \AA}^3$  compared with the  $\sim 675 \text{ \AA}^3$  molecular volume of DLPC. Furthermore, FTIR and 2D IR measurements performed on planar and vesicles bilayers with different  $W(CO)_6$  concentration demonstrated that for the concentrations used, there is no concentration dependence (*Materials and Methods*). Therefore, the presence of  $W(CO)_6$  does not have a significant influence on the global structure and dynamics of the phospholipid bilayers.

For each type of vesicle, three diameters were studied: 70, 90, and 125 nm. The data for the DLPC vesicles are also compared with those from DLPC planar bilayers (30). The results show that as the size of the vesicle is decreased, the structural fluctuations become faster. The changes with size are more pronounced for DPPC (16 carbon chains) than for DLPC (12 carbon chains). As the diameter of the DLPC vesicles increase, the dynamics approach those of the DLPC planar bilayers.

In solution chemistry, the solvent plays an important role. Solvent dynamics induce structural fluctuations in reactants that can take them to a transition state. Although proteins are very large molecules, they also undergo fast structural fluctuations (31) that can be intimately involved in processes such as enzymatic reactions (32). For cytosolic proteins, water is the solvent bath, and structural fluctuations of cytosolic proteins are coupled to water dynamics. In MD simulations of cytosolic proteins, reasonably accurate water simulation models are used to provide the simulation bath for the investigation of the proteins. Using good water models is possible because there are a large number of high-quality water simulation models that have been tested against direct measurements of water structural dynamics made with vibrational echo spectroscopy (33, 34). For the portion of a transmembrane protein that resides in the membrane, the membrane itself is the solvent bath. The 2D IR experiments presented here on vesicles and previously on planar bilayers (30) are the equivalent to those that delineated the dynamics of water (33–35).

## Results and Discussions

**IR Absorption Spectroscopy.** Fig. 1 displays the IR absorption spectra of the antisymmetric CO stretch of  $W(CO)_6$  in DLPC (Fig. 1A) and DPPC (Fig. 1B) vesicles of different sizes and DLPC planar bilayer (Fig. 1A). Because  $W(CO)_6$  is a hydrophobic molecule, it principally locates in the alkane part of phospholipid bilayer. The peak of the spectra is at  $\sim 1,982 \text{ cm}^{-1}$ . The spectra fall rapidly on the high-frequency side (blue side), but there is a long tail to the red. The tails have larger amplitude in the DLPC spectra than in the DPPC spectra. For DLPC, the three vesicle spectra are on top of each other. The

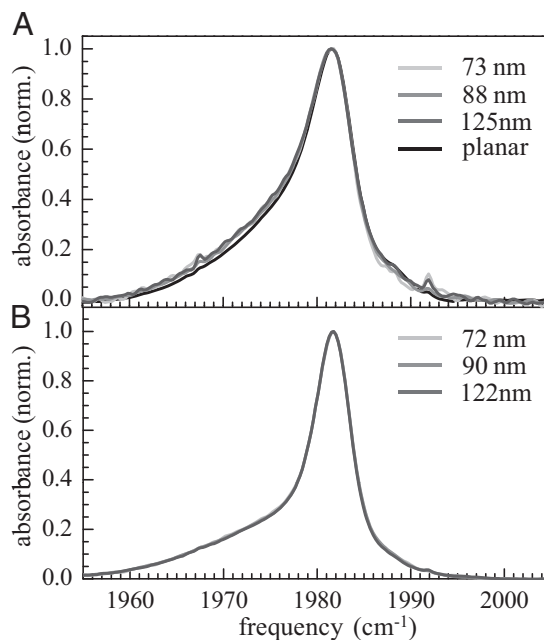


**Fig. 1.** (A) FTIR absorption spectra of the CO antisymmetric stretching mode of  $W(CO)_6$  in 73-, 88-, and 125-nm vesicles and planar DLPC bilayers and (B) in 72-, 90-, and 122-nm DPPC vesicles.

planar bilayer spectrum shows a slight difference, but this difference is probably experimental error arising from the difficulty of background subtraction for the multi-bilayer samples. For DPPC, the three spectra for the vesicles are indistinguishable. However, it was not possible to align the planar DPPC bilayers bilayer with more than 22 water molecules per lipid with high enough quality to perform the FTIR and 2D IR experiments.

As has been shown in considerable detail earlier (30), the spectrum around the maximum and on the blue side of the line originates from  $W(CO)_6$  located in the alkyl portion of the bilayers, whereas the red wing comes from the  $W(CO)_6$  interacting with the ester moieties of phospholipids. The determination of the location of the  $W(CO)_6$  in the bilayers was made by comparing its spectra in a pure alkane (a narrow peak) and in a model compound that has a diester moiety and alkyl chains but no ionic head group (a broad red-shifted band) to spectra in bilayers. The spectra in the bilayers can be quantitatively reproduced by the sum of the  $W(CO)_6$  spectra in the alkane and in the model compound (30). Therefore, the spectroscopic studies demonstrate that the peak of the spectra at  $\sim 1,982 \text{ cm}^{-1}$  arises from  $W(CO)_6$  located in the alkyl regions of the bilayers, whereas the broad wing is caused by a fraction of the  $W(CO)_6$  in the ester regions of the bilayers.

In Fig. 1, the smaller red wing for DPPC compared with DLPC shows that there is less tendency for  $W(CO)_6$  to interact with the ester groups in the DPPC vesicles. DPPC phospholipids have longer alkane chains than DLPC, which probably accounts for decreased fraction of  $W(CO)_6$  that interacts with the ester regions. For both DLPC and DPPC vesicles, the shapes of the FTIR spectra do not depend on the size of the vesicles.

The shape of  $W(CO)_6$  FTIR spectrum is very sensitive to structural changes in the bilayer (30) and the lack of change in the absorption spectra with vesicle size indicates that the structure of the bilayers does not depend on or only slightly depends on the curvature. As discussed in the Introduction, there is no consensus about size effects on vesicle bilayer structural properties.

**Table 1. FFCF (Eq. 1) and vibrational lifetime ( $T_{1a}$  and  $T_{1b}$ ) parameters for DPPC and DLPC vesicles of different sizes and DLPC planar multi-bilayers**

Sample, nm	$\Gamma$ , $\text{cm}^{-1}$	$T_2$ , ps	$\Delta_1$ , $\text{cm}^{-1}$	$\tau_1$ , ps	$\Delta_2$ , $\text{cm}^{-1}$	$\tau_2$ , ps	$T_{1a}$ , ps	$T_{1b}$ , ps
DPPC								
72	$3.4 \pm 0.3$	$3.1 \pm 0.2$	$0.8 \pm 0.1$	$2.8 \pm 0.3$	$1.1 \pm 0.1$	$17.0 \pm 0.7$	$120 \pm 4$	$41 \pm 6$
90	$3.3 \pm 0.3$	$3.1 \pm 0.3$	$1.0 \pm 0.1$	$4.3 \pm 0.4$	$1.0 \pm 0.1$	$23.2 \pm 1.3$	$116 \pm 8$	$42 \pm 5$
122	$3.2 \pm 0.2$	$3.2 \pm 0.2$	$1.1 \pm 0.1$	$5.3 \pm 0.4$	$0.9 \pm 0.1$	$30.6 \pm 3$	$117 \pm 6$	$40 \pm 4$
DLPC								
73	$3.1 \pm 0.3$	$3.4 \pm 0.3$	$1.0 \pm 0.1$	$4.1 \pm 0.4$	$1.1 \pm 0.1$	$26.4 \pm 1.9$	$110 \pm 4$	$36 \pm 5$
88	$3.0 \pm 0.2$	$3.5 \pm 0.3$	$1.1 \pm 0.1$	$4.9 \pm 0.3$	$1.0 \pm 0.1$	$31.8 \pm 2.1$	$114 \pm 4$	$32 \pm 6$
125	$3.0 \pm 0.3$	$3.5 \pm 0.2$	$1.3 \pm 0.1$	$6.4 \pm 0.4$	$0.9 \pm 0.1$	$33.2 \pm 2.7$	$109 \pm 4$	$36 \pm 4$
Planar	$2.9 \pm 0.3$	$3.6 \pm 0.4$	$1.2 \pm 0.2$	$7.5 \pm 0.4$	$0.9 \pm 0.1$	$35.4 \pm 2$	$110 \pm 3$	$37 \pm 6$

The  $\Delta$ s are SDs. The total in-homogeneous linewidth is the convolution of the two Gaussian contributions, i.e.,  $(\Delta_1^2 + \Delta_2^2)^{1/2}$ . The in-homogeneous FWHM is obtained by multiplying this number by 2.35. The total linewidth (FWHM) is the total in-homogeneous FWHM convolved with the homogeneous Lorentzian component FWHM,  $\Gamma$ .

**Time-Resolved IR Spectroscopy.** In the 2D IR experiments (36), the mid-IR pulse, tuned to the peak of the absorption spectrum (Fig. 1), was split into a weaker probe pulse and a stronger pulse. The weak pulse is routed through a mechanical delay line, which is used to set the waiting time  $T_w$ , the time between pulses 2 and 3 in the vibrational echo pulse sequence. The strong pulse was sent to a mid-IR Fourier-domain pulse shaper (36). The output from the pulse shaper, which produces pulses 1 and 2 in the vibrational echo pulse sequence, was crossed in the sample with the weak probe pulse, pulse 3. After the sample, the probe is sent into a spectrograph equipped with a 32-element mercury cadmium telluride IR array detector. The delay time between pulses 1 and 2 is  $\tau$ . The vibrational echo signal is emitted following the third pulse at a time  $\leq \tau$ , and is also heterodyned by the third pulse (36, 37). The heterodyned vibrational echo signal is then dispersed in the spectrograph, which yields the  $\omega_m$  (vertical axis) in the 2D spectrum. Scanning  $\tau$  produces a time domain interferogram at each  $\omega_m$ . These interferograms are Fourier transformed and yield the  $\omega_\tau$  (horizontal) axis of the 2D spectrum. In the experiments,  $\tau$  is scanned for fixed  $T_w$  to produce a 2D IR spectrum.  $T_w$  is then changed, and  $\tau$  is again scanned to give another 2D IR spectrum. The change in the shapes of the spectra with  $T_w$  provides the information on the structural dynamics.

When the time  $T_w$  is increased, the vibrational probe has more time to sample different structural configurations of the membrane. As a membrane's internal structure evolves, the frequency of the  $\text{W}(\text{CO})_6$  stretch changes within the distribution of frequencies reflected in the inhomogeneously broadened absorption spectrum. This frequency evolution is called "spectral diffusion." Spectral diffusion is directly related to the conformational fluctuations of the membrane. The time dependence of the spectral diffusion was extracted from the 2D IR spectra using center line slope (CLS) formalism (38, 39). The CLS method quantifies the time-dependent changes in 2D line shapes, and is used to obtain the frequency-frequency correlation function (FFCF). The CLS is a normalized function that is closely related to the FFCF. Its decay times are the same as those in the FFCF. The difference between 1 and the value of the CLS at  $T_w = 0$  is related to the homogeneous component of the dynamic spectral line. Combining the CLS with the linear absorption spectrum allows the full FFCF to be obtained. The FFCF is the direct connection between the experimental observables and the details of the dynamics and structure of the system.

A multiexponential form of the FFCF,  $C(t)$ , was used to model the FFCF (33, 38, 39):

$$C(t) = \sum_{i=1}^n \Delta_i^2 e^{-t/\tau_i} \quad [1]$$

For the  $i^{\text{th}}$  dynamical process,  $\Delta_i$  is the range of frequencies sampled due to fluctuations of the  $\text{W}(\text{CO})_6$  environment and  $\tau_i$  is the time constant associated with these fluctuations. If  $\Delta_i \tau_i < 1$ , the dynamics are motionally narrowed and contribute to the homogeneous linewidth. The motionally narrowed dynamics are characterized by  $T_2^* = 1/\Delta_i^2 \tau_i$ , where  $T_2^*$  is the pure dephasing time.  $T_2^*$  is the result of ultrafast structural fluctuations, typically with time scales  $< 100$  fs. The total homogeneous dephasing time,  $T_2$ , is given by  $1/T_2 = 1/T_2^* + 1/2T_1 + 1/3T_{\text{or}}$ . The homogeneous linewidth is  $\Gamma = 1/\pi T_2$ .  $T_1$  is the vibrational lifetime and  $T_{\text{or}}$  is the orientational relaxation time, both of which were measured by IR pump-probe experiments. All of the homogeneous dephasing linewidths are  $\sim 3 \text{ cm}^{-1}$  (Table 1). The vibrational lifetimes are long ( $\sim 120$  ps, Table 1) and therefore contribute a negligible amount ( $\sim 0.05 \text{ cm}^{-1}$ ) to the homogeneous linewidths. The orientational relaxation times are all  $\sim 6$  ps. The orientational relaxation contributes  $\sim 0.6 \text{ cm}^{-1}$  to the homogeneous linewidth. This is a small contribution that does not vary systematically with the sample. The homogeneous linewidths reported in Table 1 contain all contributions but are dominated by pure dephasing.

Two-dimensional IR vibrational echo spectra of the antisymmetric CO stretch of  $\text{W}(\text{CO})_6$  in 72-nm diameter DLPC vesicles are shown in Fig. 2 at  $T_w = 0.3$  ps (Fig. 2, Upper) and  $T_w = 42$  ps (Fig. 2, Lower). The dashed line in Fig. 2, Upper is the diagonal. At short time, the 2D spectrum is elongated along the diagonal. Spectral diffusion causes the shape to become more symmetrical. In Fig. 2, Lower, the change in shape is evident. Many 2D spectra were measured for DLPC and DPPC vesicles of different sizes. The changes in shape with increasing  $T_w$  were quantified with the CLS method (38, 39). The CLSs were determined around the peaks of the spectra, which eliminates influence from the red wing of the absorption spectrum (30). Therefore, the results presented below are for the  $\text{W}(\text{CO})_6$  located in the alkyl region of the bilayers, and do not have contribution from the ester region.

Fig. 3 displays CLS decay curves for the antisymmetric stretch of  $\text{W}(\text{CO})_6$  in DPPC vesicles of different sizes (Fig. 3, circles) and fits to the data (Fig. 3, solid curves). All of the DPPC data as well as the data from DLPC vesicles fit exceedingly well to biexponential decay functions. The FFCF parameters determined by simultaneous fit of CLS decays and FTIR spectra are listed in Table 1. First consider the DPPC vesicle results. The homogeneous linewidths,  $\Gamma$ , and the related homogeneous dephasing times,  $T_2$ , are the same within experimental error.  $\Gamma$  is dominated by pure dephasing, which arises from ultrafast

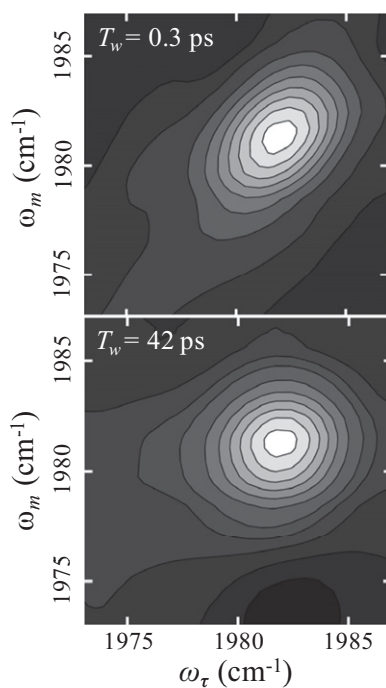


**Fig. 2.** Two-dimensional IR vibrational echo spectra of the CO antisymmetric stretching mode of  $W(\text{CO})_6$  in DLPC vesicle bilayers 72 nm in diameter at short  $T_w = 0.3$  ps (Upper) and long  $T_w = 42$  ps (Lower). The change in 2D line shape with time reveals the time dependence of spectral diffusion which is caused by the structural dynamics of the bilayer.

motions, which are probably associated with librations; they do not change with the size of the vesicle. In contrast with the homogeneous dephasing, the two spectral diffusion time constants,  $\tau_1$  and  $\tau_2$ , vary systematically with size. As the vesicle becomes larger, both time constants become slower. The changes in both time constants are approximately a factor of 2 going from 72 to 122 nm in diameter. These time constants reflect the time scales for randomization of the structures in the interior alkyl regions of the bilayer that give rise to the inhomogeneously broadened absorption line. The amplitude factors,  $\Delta_1$  and  $\Delta_2$ , do not change significantly with size, which shows the partitioning of the dynamics between faster and slower structural motions does not change with size.

The FFCF parameters for DLPC (Table 1) display the same trends with size as observed for the DPPC vesicles. However, the spectral diffusion dynamics ( $\tau_1$  and  $\tau_2$ ) in DLPC are slower than those in DPPC. In addition, for DLPC we were able to obtain the FFCF parameters for planar bilayers that are fully hydrated and at the same temperature used for the vesicle experiments (Table 1) (30). The time constants,  $\tau_1$  and  $\tau_2$ , are slower in the planar bilayer than they are for the largest DLPC vesicles, 125 nm. As the vesicles become larger, the dynamics approach the values found for planar bilayers.

The vibrational lifetimes of the antisymmetric stretch of  $W(\text{CO})_6$  in the various samples were also measured. As discussed in connection with Fig. 1 and analyzed in detail previously, the red wing in the FTIR spectra arise from a fraction of the  $W(\text{CO})_6$  residing in proximity to the ester groups. The 2D IR data are from the alkyl region of the spectrum, and it was not possible to obtain 2D IR data on the red wing because it is broad and low amplitude. However, we were able to measure the vibrational lifetimes at the peaks of the spectra ( $T_{1a}$ , alkyl region) and in the red wing ( $T_{1e}$ , ester region). The results are shown in the last two columns of Table 1. The vibrational lifetime is very sensitive to the local environment of the relaxing vibrational oscillator. As can be seen in

Table 1, there is a large difference, approximately a factor of 3, in the alkyl regions vs. ester regions of the bilayers. For each region of DPPC, the lifetimes are independent of the vesicle size. The same is true for DLPC, but the lifetimes in both regions are shorter than those in DPPC, which demonstrates a difference in the immediate environment experienced by the IR probe that depends on chain length. These results indicate that for a given phospholipid, there is no substantial change in local structure as the size of the vesicle is changed. Although the immediate environment may not change with the vesicle size, the 2D IR results show that the more global structural dynamics are sensitive to the radius of curvature.

At this time we do not have a definite reason why the structural dynamics in the bilayers become faster as the diameters of the vesicles decrease. Because the experiments are observing dynamics deep in the alkyl regions of the bilayers, it is unlikely that a change in water penetration with a change in size is responsible for the differences. The extent of water in the region near the bilayer–water interface may change with vesicle diameter. The amount of water residing in the DLPC bilayers below the bilayer–water interface will change with the level of hydration. The  $W(\text{CO})_6$  spectrum in planar DLPC changed substantially with the level of hydration of the head groups in the range from two-water-molecules-per-head group to fully hydrated, i.e., 16 waters, but the dynamics in the alkyl region did not change (30). In the study of the DLPC vesicles and the DPPC vesicles, the  $W(\text{CO})_6$  spectra do not change with vesicle size. Therefore, the extent of water penetration into the bilayers is unlikely to be involved in the changes in dynamics measured with the 2D IR experiments.

In going from a planar bilayer to smaller and smaller vesicles, the structure of the alkyl region of the bilayers must change. For planar bilayers, at the interior interface, that is, the region where the alkyl chains from one leaflet meet those from the other leaflet, the chains from the two leaflets will have the same average structure. For a planar bilayer, there is the same number of lipid molecules in the two leaflets. Although there will be considerable disorder at this interior interface, the surface area per pair of alkyl chains from a given lipid molecule will be the same for both leaflets. This is not the case for a vesicle. In vesicles, the interior spherical interface has a smaller diameter than that of the surface of the outer leaflet but a larger diameter than the surface of the inner leaflet. The outer leaflet has more lipid molecules than the inner leaflet. Therefore, at the interior interface, alkyl chains of the inner leaflet will have more surface area than those from the outer leaflet. As the vesicles become

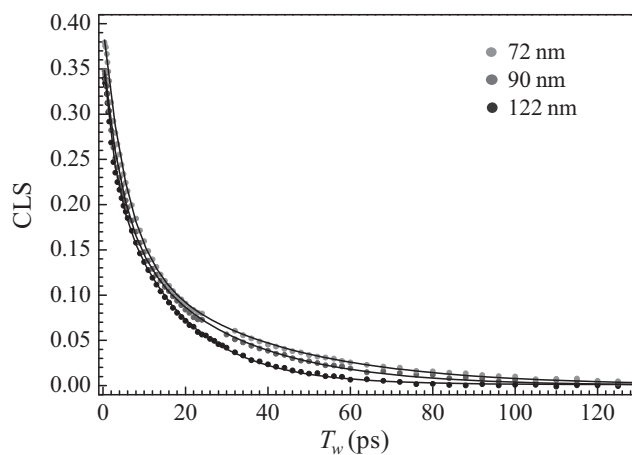


**Fig. 3.** CLS decay curves obtained from the 2D IR spectra of the CO antisymmetric stretching mode of  $W(\text{CO})_6$  in 72-, 90-, and 122-nm DPPC vesicle bilayers (points) and biexponential fits (solid curves).

smaller, the difference in area per lipid alkyl chain pair for the outer and inner leaflet increases.

To obtain a feel for this difference in area with size, a simple model can be used. Assume that the thickness of the inner and outer leaflets is the same and that the area of the lipid head groups for the inner and outer leaflets is the same. With these assumptions it is straightforward to derive expressions for the ratio of the chain pair area at the interior interface of the vesicle outer leaflet to the planar chain pair area,  $R_{out}$ , and the ratio of the chain pair area of the vesicle inner leaflet to the planar chain pair area,  $R_{in}$ .  $R_{out} = 1 - \gamma/r_v$  and  $R_{in} = (r_v - \gamma)/(r_v - 2\gamma)$ .  $r_v$  is the vesicle radius and  $\gamma$  is the bilayer thickness. Note that in these formulas, when  $r_v$  goes to infinity, the ratio goes to 1, as it should. For DPPC  $\gamma = 3.9$  nm, and for DLPC  $\gamma = 3.1$  nm (40). The diameters of the vesicles are given in Table 1. For DPPC the values for large to small vesicles,  $(R_{in}, R_{out}) = (1.07, 0.94)$ ,  $(1.11, 0.91)$ , and  $(1.14, 0.89)$ . For DLPC the values for large to small vesicles,  $(R_{in}, R_{out}) = (1.06, 0.95)$ ,  $(1.08, 0.93)$ , and  $(1.10, 0.92)$ . In each case, as the diameter of the vesicles becomes smaller, the difference between  $R_{in}$  and  $R_{out}$  becomes bigger. In addition, these differences in ratios are less pronounced for DLPC than for DPPC. The trend of the ratios is in line with the trend of the dynamical data. As the diameter becomes smaller, the dynamics become faster. The changes in dynamics are greater for DPPC than for DLPC. For DLPC, we also have the dynamical data for the planar bilayer that can be compared with  $(R_{in}, R_{out}) = (1, 1)$ . The planar bilayer dynamics are slower than those of the largest vesicle.

Although the interior interface of the two leaflets will not be smooth, and there will be intercalation of the chains from the outer leaflet into the voids from the inner leaflet, the nature of the chain structure in the alkyl region will clearly be distinct from that of a planar bilayer. The ratios given above suggest that the changes in chain structure will increase with decreasing vesicle diameter. The result can be faster alkyl chain structural fluctuations, which give rise to the faster spectral diffusion as the vesicle size decreases (Table 1). MD simulations would be extremely useful in identifying the differences in structure and the associated changes in dynamics suggested by the ratios given above.

## Concluding Remarks

In this article we presented a study of the ultrafast structural dynamics inside of phospholipid vesicles of different sizes. The experiments directly measure the time dependence of structural fluctuations of the alkyl interior of the bilayers using 2D IR vibrational echo experiments. The hydrophobic  $W(CO)_6$  vibrational probe, which has a long vibrational lifetime, was used to monitor structural dynamics in the time window of 300 fs to 200 ps in vesicle and planar phospholipid bilayers. The results presented here provide strong experimental evidence that the alkyl region structural dynamics depend on the size of the vesicles and the chain lengths of the lipids. A decrease in vesicle diameter from 125 to 70 nm results in faster bilayer structural dynamics. This change is more pronounced for vesicles formed from longer alkyl chain length DPPC phospholipids than for DLPC lipids. In addition, for DLPC it was possible to compare the vesicle structural dynamics with those of planar bilayers under the same hydration and temperature conditions. It was observed that as the vesicles became larger, the dynamics approach those of the planar bilayers. However, even vesicles with diameters of 125 nm still display faster dynamics than those observed for the planar bilayers.

In cells, the membrane is the solvent for transmembrane proteins. The structural fluctuations of membranes couple to the

structural dynamics of proteins and enzymes and will influence processes such as transport through ion channels and chemical reactions. Cells are relatively large. Eukaryotic cells range in size from 10 to 30  $\mu\text{m}$ . The membranes of such cells, although not perfectly planar, are nearly so. In contrast, large vesicles are  $\sim 100$  nm in diameter, and many experiments on membrane-bound proteins are conducted in much smaller vesicles. For many types of experiments, the results presented here that the dynamics of vesicle bilayers and particularly small vesicle bilayers are significantly faster than those in planar bilayers will not matter. However, experiments that address dynamical processes, even processes that are slow overall, can be affected by the differences in vesicle dynamics compared with planar bilayers.

## Materials and Methods

**Sample Preparation.** Lipids were obtained from Avanti Polar Lipids and  $W(CO)_6$ ,  $D_2O$ , and dichloromethane were purchased from Sigma-Aldrich. All chemicals were used as received. Vesicles were prepared by the extrusion method using an Avanti miniextruder. The lipid/ $W(CO)_6$  mixture was first dissolved in dichloromethane, the dichloromethane was evaporated, and the lipid was rehydrated in  $D_2O$ . The concentration of  $W(CO)_6$  in the bilayers was small, with 1  $W(CO)_6$  per 800 lipid molecules in the planar bilayers and 1 per 100 in the vesicles. For the planar systems, FTIR and 2D IR measurements were also made with both 1 per 400 and 1 per 200. For all of these concentrations, the results were the same. For the vesicles, FTIR measurements were made from 1 to 100 down to 1 to 800, and the spectra were unchanged. In addition, the 2D IR measurements were made on 1 to 200 samples, which gave the identical results as the 1 to 100 samples.

The lipid/ $W(CO)_6/D_2O$  solution was heated above the lipid phase transition temperature, vortexed, and extruded through a polycarbonate filtering membrane of 30-, 50-, or 100-nm pore sizes. The vesicle sizes were measured by dynamic light scattering. Planar lipid bilayers with  $W(CO)_6$  were aligned between two  $CaF_2$  windows with a 75- $\mu\text{m}$  spacer as described earlier (30). The temperature was kept at 45  $^\circ\text{C}$  for DLPC and DPPC vesicles and DLPC bilayers.

**FTIR Spectroscopy.** All FTIR spectra were measured with 0.5  $\text{cm}^{-1}$  resolution. Spectra without  $W(CO)_6$  were collected and subtracted from the spectra with  $W(CO)_6$  to obtain the spectra without background.

**Dynamic Light Scattering.** The sizes of the vesicles were determined using a NanoBrook 90Plus (Brookhaven Instruments Corporation) light-scattering instrument using the Particle Sizing Software with the Zeta Pals option. All measurements were performed on freshly prepared vesicles at a temperature of 45  $^\circ\text{C}$ .

**Two-Dimensional IR Vibrational Echo Spectroscopy.** The output of a Ti:Sapphire oscillator/regen operating at 1 kHz with a pulse energy of  $\sim 700$   $\mu\text{J}$  and duration of  $\sim 100$  fs was used to pump a mid-IR optical parametric amplifier (OPA). The output of the OPA was centered at  $\sim 1,980$   $\text{cm}^{-1}$  with a 170-fs duration and  $\sim 8$   $\mu\text{J}$  pulses, and used for the 2D IR (*Results and Discussion*) and IR pump-probe experiments. The pump-probe experiments were performed with the pump pulse polarization at the magic angle relative to the probe, which gives the vibrational lifetime, and with the pump and probe pulses having the same polarization, which gives a combination of the orientational relaxation and the vibrational lifetime. Using the lifetime from the magic angle experiments, the orientational relaxation times were obtained (30).

**ACKNOWLEDGMENTS.** We thank Laura Hughes and Bob Rawle for help with vesicle extrusion. A.T. thanks the Stanford Graduate Fellowships Program for a fellowship. This work was funded by the Division of Chemical Sciences, Geosciences, and Biosciences, Office of Basic Energy Sciences of the US Department of Energy through Grant DE-FG03-84ER13251 and by the Division of Chemistry, Directorate of Mathematical and Physical Sciences, National Science Foundation Grant CHE-1157772 for partial support (to O.K.) and partial support of the equipment used in experiments.

1. Janmey PA, Kinnunen PKJ (2006) Biophysical properties of lipids and dynamic membranes. *Trends Cell Biol* 16(10):538–546.
2. Lee AG (2004) How lipids affect the activities of integral membrane proteins. *Biochim Biophys Acta* 1666(1-2):62–87.

3. McIntosh TJ, Simon SA (2006) Roles of bilayer material properties in function and distribution of membrane proteins. *Annu Rev Biophys Biomol Struct* 35:177–198.
4. Jensen MØ, Mouritsen OG (2004) Lipids do influence protein function—the hydrophobic matching hypothesis revisited. *Biochim Biophys Acta* 1666(1-2):205–226.

5. Bienvenie M, Marie JS (1994) Modulation of protein function by lipids. *Curr. Top. Membr.* 40:319–354.
6. Kucerka N, Pencic J, Sachs JN, Nagle JF, Katsaras J (2007) Curvature effect on the structure of phospholipid bilayers. *Langmuir* 23(3):1292–1299.
7. Risselada HJ, Marrink SJ (2009) Curvature effects on lipid packing and dynamics in liposomes revealed by coarse grained molecular dynamics simulations. *Phys Chem Chem Phys* 11(12):2056–2067.
8. Kiselev MA, Zemlyanaya EV, Aswal VK, Neubert RHH (2006) What can we learn about the lipid vesicle structure from the small-angle neutron scattering experiment? *Eur Biophys J* 35(6):477–493.
9. Schmiedel H, Almásy L, Klose G (2006) Multilamellarity, structure and hydration of extruded POPC vesicles by SANS. *Eur Biophys J* 35(3):181–189.
10. Lin CM, Li CS, Sheng YJ, Wu DT, Tsao HK (2012) Size-dependent properties of small unilamellar vesicles formed by model lipids. *Langmuir* 28(1):689–700.
11. Huang C, Mason JT (1978) Geometric packing constraints in egg phosphatidylcholine vesicles. *Proc Natl Acad Sci USA* 75(1):308–310.
12. Brzustowicz MR, Brunger AT (2005) X-ray scattering from unilamellar lipid vesicles. *J Appl Cryst* 38:126–131.
13. Zhu T, Jiang ZY, Ma YQ (2012) Lipid exchange between membranes: Effects of membrane surface charge, composition, and curvature. *Colloids Surf B Biointerfaces* 97:155–161.
14. Shintani M, Yoshida K, Sakuraba S, Nakahara M, Matubayasi N (2011) NMR-NOE and MD simulation study on phospholipid membranes: dependence on membrane diameter and multiple time scale dynamics. *J Phys Chem B* 115(29):9106–9115.
15. Bocian DF, Chan SI (1978) NMR-studies of membrane structure and dynamics. *Annu Rev Phys Chem* 29:307–335.
16. Parmar YI, Wassall SR, Cushley RJ (1984) Orientational order in phospholipid bilayers. Deuterium NMR study of selectively deuterated palmitic acids in unilamellar vesicles. *J Am Chem Soc* 106(8):2434–2435.
17. Yokoyama H, Ikeda K, Wakabayashi M, Ishihama Y, Nakano M (2013) Effects of lipid membrane curvature on lipid packing state evaluated by isothermal titration calorimetry. *Langmuir* 29(3):857–860.
18. Nir S, Wilschut J, Bentz J (1982) The rate of fusion of phospholipid vesicles and the role of bilayer curvature. *Biochim Biophys Acta* 688(1):275–278.
19. Ahmed S, Wunder SL (2009) Effect of high surface curvature on the main phase transition of supported phospholipid bilayers on SiO<sub>2</sub> nanoparticles. *Langmuir* 25(6):3682–3691.
20. Rutkowski CA, Williams LM, Haines TH, Cummins HZ (1991) The elasticity of synthetic phospholipid vesicles obtained by photon correlation spectroscopy. *Biochemistry* 30(23):5688–5696.
21. Asher SA, Pershan PS (1979) Alignment and defect structures in oriented phosphatidylcholine multilayers. *Biophys J* 27(3):393–421.
22. Kucerka N, et al. (2005) Structure of fully hydrated fluid phase DMPC and DLPC lipid bilayers using X-ray scattering from oriented multilamellar arrays and from unilamellar vesicles. *Biophys J* 88(4):2626–2637.
23. McMahon HT, Kozlov MM, Martens S (2010) Membrane curvature in synaptic vesicle fusion and beyond. *Cell* 140(5):601–605.
24. Lentz BR, Barenholz Y, Thompson TE (1976) Fluorescence depolarization studies of phase transitions and fluidity in phospholipid bilayers. 2. Two-component phosphatidylcholine liposomes. *Biochem* 15(20):4529–4537.
25. Brumm T, Jørgensen K, Mouritsen OG, Bayerl TM (1996) The effect of increasing membrane curvature on the phase transition and mixing behavior of a dimyristoyl-sn-glycero-3-phosphatidylcholine/distearoyl-sn-glycero-3-phosphatidylcholine lipid mixture as studied by Fourier transform infrared spectroscopy and differential scanning calorimetry. *Biophys J* 70(3):1373–1379.
26. Lepore LS, Ellena JF, Cafiso DS (1992) Comparison of the lipid acyl chain dynamics between small and large unilamellar vesicles. *Biophys J* 61(3):767–775.
27. Bloom M, et al. (1978) Fatty acyl chain order in lecithin model membranes determined from proton magnetic resonance. *Biochemistry* 17(26):5750–5762.
28. Korstanje LJ, van Faassen EE, Levine YK (1989) Reorientational dynamics in lipid vesicles and liposomes studied with ESR: Effects of hydration, curvature and unsaturation. *Biochim Biophys Acta* 982(2):196–204.
29. Stockton GW, Polnaszek CF, Tulloch AP, Hasan F, Smith ICP (1976) Molecular motion and order in single-bilayer vesicles and multilamellar dispersions of egg lecithin and lecithin-cholesterol mixtures. A deuterium nuclear magnetic resonance study of specifically labeled lipids. *Biochemistry* 15(5):954–966.
30. Kel O, Tamimi A, Thielges MC, Fayer MD (2013) Ultrafast structural dynamics inside planar phospholipid multibilayer model cell membranes measured with 2D IR spectroscopy. *J Am Chem Soc* 135(30):11063–11074.
31. Bagchi S, Nebgen BT, Loring RF, Fayer MD (2010) Dynamics of a myoglobin mutant enzyme: 2D IR vibrational echo experiments and simulations. *J Am Chem Soc* 132(51):18367–18376.
32. Thielges MC, Chung JK, Fayer MD (2011) Protein dynamics in cytochrome P450 molecular recognition and substrate specificity using 2D IR vibrational echo spectroscopy. *J Am Chem Soc* 133(11):3995–4004.
33. Asbury JB, et al. (2004) Dynamics of water probed with vibrational echo correlation spectroscopy. *J Chem Phys* 121(24):12431–12446.
34. Asbury JB, et al. (2004) Water dynamics: Vibrational echo correlation spectroscopy and comparison to molecular dynamics simulations. *J Phys Chem A* 108(7):1107–1119.
35. Fecko CJ, Eaves JD, Loparo JJ, Tokmakoff A, Geissler PL (2003) Local and collective hydrogen bond dynamics in the ultrafast vibrational spectroscopy of liquid water. *Science* 301:1698–1702.
36. Karthick Kumar SK, Tamimi A, Fayer MD (2012) Comparisons of 2D IR measured spectral diffusion in rotating frames using pulse shaping and in the stationary frame using the standard method. *J Chem Phys* 137(18):184201.
37. Shim S-H, Zanni MT (2009) How to turn your pump-probe instrument into a multidimensional spectrometer: 2D IR and Vis spectroscopies via pulse shaping. *Phys Chem Chem Phys* 11(5):748–761.
38. Kwak K, Park S, Finkelstein IJ, Fayer MD (2007) Frequency-frequency correlation functions and apodization in 2D-IR vibrational echo spectroscopy, a new approach. *J Chem Phys* 127:124503.
39. Kwak K, Rosenfeld DE, Fayer MD (2008) Taking apart 2D-IR vibrational echo spectra: More information and elimination of distortions. *J Chem Phys* 128:204505.
40. Kučerka N, Nieh MP, Katsaras J (2011) Fluid phase lipid areas and bilayer thicknesses of commonly used phosphatidylcholines as a function of temperature. *Biochim Biophys Acta* 1808(11):2761–2771.